The Xe-Cl_2 Conundrum: van der Waals Complex or Linear Molecule?

Davide M. Proserpio,[†] Roald Hoffmann,*[,†] and Kenneth C. Janda[‡]

Contribution from the Department of Chemistry and Materials Science Center, Cornell University, Ithaca, New York 14853-1301, and Department of Chemistry, University of Pittsburgh, Pittsburgh, Pennsylvania 15260. *Received March 20, 1991*

Abstract: We present an approximate molecular orbital analysis of the potential energy surface for $XeCl_2$, supported by qualitative perturbation theoretic analysis of the bonding in these species. Three minima are located on the $XeCl_2$ surface: the observed Xe···Cl_2 van der Waals complex, the linear Cl-Xe-Cl molecule, and between them an unexpected strongly bent ClXeCl intermediate. The latter is characterized by a qualitatively different electronic configuration and is likely to have barriers between it and the two other potential minima. Possible experimental methods to observe both the intermediate geometry and the linear molecule are discussed. The reaction pathway for the conversion of the van der Waals isomer of $XeCl_2$ to the more stable linear isomer passes through the newly predicted bent isomer and thus proceeds through two curve-crossing regions. This explains why the van der Waals isomer can be observed in the gas phase.

Introduction

An intriguing problem, at the interface of noble-gas chemistry and modern spectroscopy, has arisen around the possible molecular species of stoichiometry $XeCl_2$.

Since the discovery of the xenon fluorides, several attempts have been made to isolate the analogous chlorides. Xenon dichloride was first observed[1] in the condensed products of a xenon–chloride microwave discharge[2,3] and in the β-decay reaction $^{129}ICl_2^- \rightarrow {}^{129}XeCl_2$.[4] Further matrix isolation experiments studied the molecule trapped in solid Xe after the photolysis of embedded Cl_2.[5,6] Infrared,[25] Raman,[25] and Mössbauer[4] spectroscopies suggested a linear ClXeCl geometry, in accord with molecular orbital and Xα calculations.[7]

Given the existence and known structure of XeF_2, there was nothing startling in these observations. Meanwhile, with the remarkable advances in modern laser spectroscopy, physical chemists quite naturally turned to the study of the van der Waals (vdW) complexes of various molecules in the gas phase. Detailed spectroscopic information has become available on several Ng···XY complexes (Ng = noble-gas element; X, Y = halogens).[8] For $X \neq Y$ linear complexes are observed, but for X = Y there is clear evidence for a preferred T-shaped structure, with a binding energy from 0.03 to 0.83 kcal·mol^{-1}, depending on Ng.

Until recently, there was no intersection of the older matrix isolation work on stable molecular species and the recent studies of vdW complexes. This is because the laser spectroscopy studies avoided fluorine and concentrated on the lighter noble gases. Recently, a meeting point was provided by a study of Xe···Cl_2; pump–probe experiments indicated a T-shaped complex, with only a weak, van der Waals Xe-Cl_2 bond.[9,10]

One set of experiments indicates a stable linear Cl-Xe-Cl molecule, I, and another a weakly bound van der Waals complex, II. There must be a barrier between these geometries; understanding the nature of this barrier is the object of this study.

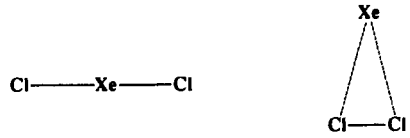

I II

In this paper we will show, using extended Hückel calculations (details are provided in the Appendix), that there are several surprises in this simple system. These approximate molecular orbital calculations are not reliable for computing quantitative potential energy surfaces, but they have proven very fruitful in isolating the orbital trends and the level crossings that are responsible for barriers or the absence thereof in chemical reactions. Such level crossings will be shown to be responsible for the predicted existence of an unexpected local minimum in the potential energy surface for $XeCl_2$.

The van der Waals Complex

We begin by comparing two possible geometries for the vdW complex: linear and T-shaped. The analysis proceeds by computation of the Walsh diagram along the distortion $C_{\infty v} \rightarrow C_s \rightarrow C_{2v}$. The Xe–Cl distance is first kept constant at 3.8 Å, a distance typical of other Ng···Cl_2 systems,[8] and the Cl_2 molecule at the equilibrium distance of 1.988 Å (III).

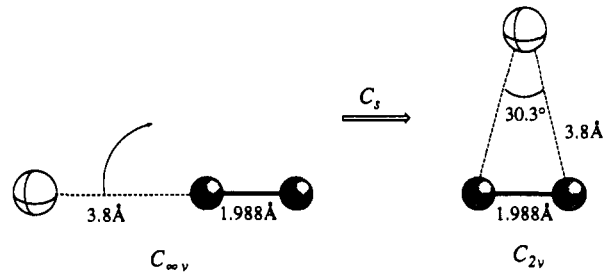

III

In Figure 1, we show the Walsh diagram for the distortion. The geometrical variation is accomplished by 11 incremental steps in the distance between Xe and the center of mass of the Cl_2 molecule, along the arc that keeps the Xe–nearest Cl separation constant at 3.8 Å. For this and the subsequent Walsh diagrams, the levels are labeled according to the symmetry preserved along the distortion (in this case C_s), with the numbering referred to

[†] Cornell University.
[‡] University of Pittsburgh.

(1) The synthesis of solid $XeCl_2$ has been reported[1a,b] without chemical analysis. Apparently no attempts to synthesize the molecule have been reported since then. Some authors suggest that the solid observed was indeed a clathrate.[1c,d] (a) Meinert, H. *Z. Chem.* **1966**, *6*, 71. (b) Kettle, S. F. A. *Chem. Ind. (London)* **1966**, 1846. (c) Malm, J. G.; Appelman, E. H. *At. Energy Rev.* **1969**, *7*, 3. (d) Neiding, A. B.; Sokolov, V. B. *Russ. Chem. Rev. (Engl. Transl.)* **1974**, *43*, 1043.
(2) Nelson, L. Y.; Pimentel, G. C. *Inorg. Chem.* **1967**, *6*, 1758.
(3) Boal, D.; Ozin, G. A. *Spectrosc. Lett.* **1971**, *4*, 43.
(4) Perlow, G. J.; Perlow, M. W. *J. Chem. Phys.* **1968**, *48*, 955.
(5) Howard, W. F.; Andrews, L. *J. Am. Chem. Soc.* **1974**, *96*, 7864.
(6) (a) Beattie, J. R.; German, A.; Blayden, H. E.; Brumbach, S. B. *J. Chem. Soc., Dalton Trans.* **1975**, 1659. (b) Qureshi, S.; Ansari, G. M. *Sind Univ. Res. J., Sci. Ser.* **1982**, *14*, 131.
(7) (a) Waters, J. H.; Gray, H. B. *J. Am. Chem. Soc.* **1963**, *85*, 825. (b) Mitchell, K. A. R. *J. Chem. Soc. A* **1969**, 1637. (c) Catton, R. C.; Mitchell, K. A. R. *Can. J. Chem.* **1970**, *48*, 2695. (d) Scheire, L.; Phariseau, P.; Nuyts, R.; Foti, A. E.; Smith, V. H., Jr. *Physica A: (Amsterdam)* **1980**, *101*, 22.
(8) Janda, K. C.; Bieler, C. R. In *Atomic and Molecular Clusters*; Bernstein, E., Ed.; Elsevier: Amsterdam, 1990; Chapter 6 and references therein.
(9) Bieler, C. R.; Janda, K. C. *J. Am. Chem. Soc.* **1990**, *112*, 2033.
(10) Bieler, C. R.; Spence, K. E.; Janda, K. C. *J. Phys. Chem.* **1991**, *95*, 5058.

0002-7863/91/1513-7184$02.50/0

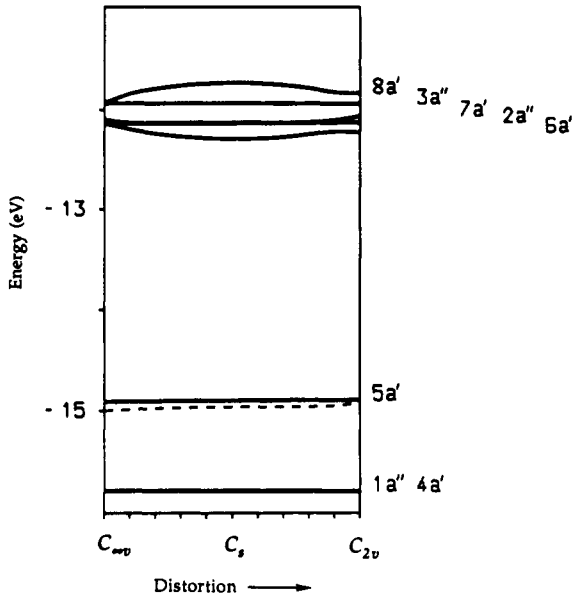

Figure 1. Walsh diagram for distortion III leading from a linear to a T-shaped van der Waals complex. The LUMO 9a', not shown, lies at an energy >-9 eV.

the starting geometry. It should be noted explicitly that our MO numbering system is designed for valence-electron calculations and does not include core orbitals. The dashed line shows the variation of the total energy of the system along the distortion, on the same scale as the levels. In this case, we get a barely noticeable preference for the linear geometry. The total-energy curve rises linearly by ~0.08 eV (1.8 kcal·mol^{-1}) from linear to T-shaped geometry.[11]

To determine whether the complex is bound, we computed a Walsh diagram for the constraint drawn in IV, where we change

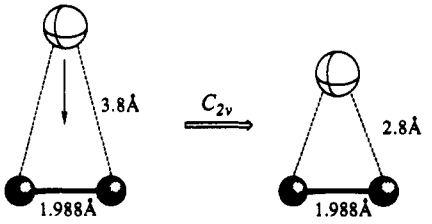

IV

the Xe–Cl separation within a C_{2v} geometry. We also produced a similar curve for the linear geometry. In neither case did we get any binding; the energy decreases as one separates Xe and Cl_2. Extended Hückel calculations do not in general give van der Waals bonding, though they capture the effects of strong donor–acceptor interactions and covalent bonding.

From the van der Waals Complex to the Molecule

Now we study a possible transformation from the T-shaped vdW complex to the linear molecule, Cl–Xe–Cl. To guide us in the search for a minimum energy path, we compute a potential energy surface defined by two parameters (see V): (a) the distance of Xe from the midpoint of the Cl–Cl line and (b) the Cl–Cl distance. The resulting surface is shown in Figure 2.

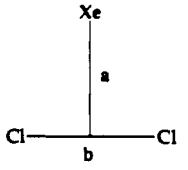

V

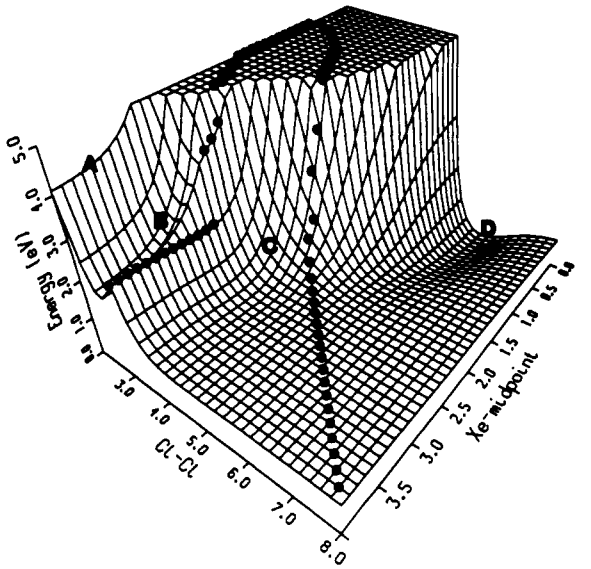

Figure 2. Potential energy surfaces for the Xe–Cl_2 system. A–D indicate the structures discussed in the text. The black dots mark the geometries at which the crucial $4b_1$–$5a_1$ level crossing discussed in the text occurs.

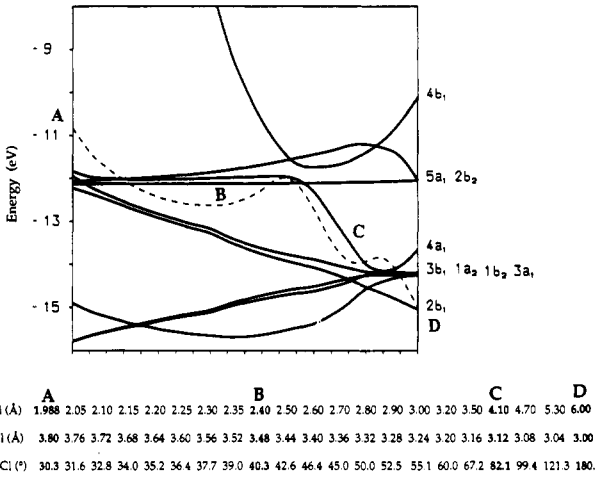

Figure 3. Walsh diagram for distortion VI (A → B → C → D), with the geometries of each step.

The global minimum on this surface corresponds to a Cl–Xe–Cl linear geometry with a computed Xe–Cl distance of 3.0 Å.[12] There are other minima on this surface, which will be demonstrated to be important, even if they are not deep.

Following the shape of the energy surface, we select a pathway to go from the T-shaped complex A to the linear molecule D. Two minima, B and C, are traversed along the way and are indicated in Figure 2. Although extended Hückel calculations should not be used to trace quantitatively a reaction path, the minima are set by level crossings, and we expect that higher level calculations will reproduce the qualitative features.

The computed Walsh diagram in Figure 3 shows the various minima and level crossings. At the bottom of Figure 3, we list the geometries of each step along the assumed reaction path. In VI, we show the geometries for the starting complex, A, and the three minima, B, C, and D.

A and B do not represent separate species. Since extended Hückel theory underestimates the Cl–Cl attraction, it gives an energy too high for structure A, which is an experimental geometry. Structure B is the closest representation of this minimum in our calculation. Thus there are two barriers that will be interesting to analyze. These barriers are due to level crossings as

(11) Similar results were reported by: Burdett, J. K. *J. Chem. Phys.* **1980**, *73*, 2825.

(12) This value is long compared to the one obtained by the other calculation.[7]

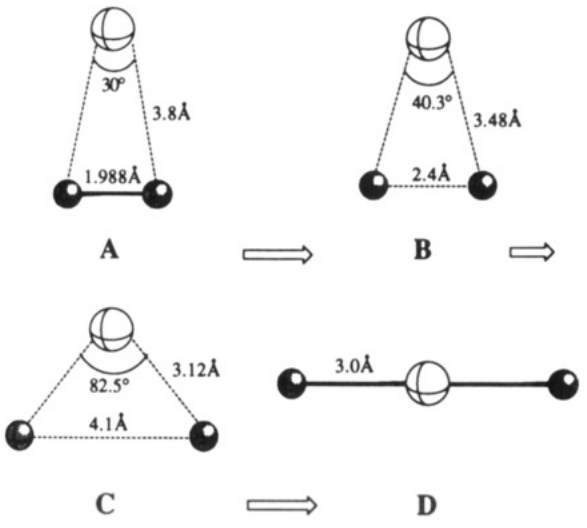

VI

the geometry changes from B to C and from C to D.

To understand the nature of the first level crossing and the associated energy barrier in moving from B to C, it is instructive to analyze the diagram for the interaction between the Xe atoms and the Cl_2 unit in the two minima (Figures 4 and 5). The molecular orbitals involved are shown in Figure 6.

We look first at the interaction diagram for complex B, Figure 4. We observe a weak interaction between Xe and Cl_2. While the Cl–Cl bond is stretched, the two chlorines are still bound to each other, as is clear from the energy separation of the levels on the right side of the diagram. The antibonding σ_u level lies high in energy and correlates, unperturbed, with the LUMO of the complex. The HOMO $5a_1$ and the level immediately below, $3b_1$ (second HOMO), are the antibonding components of the interaction between the p_z and p_x orbitals of Xe and two MOs from the π_u and π_g orbitals of Cl_2. The shape of these three MOs is indicated in Figure 6 (left).

Moving from B to C, the interaction between the two Cl atoms is almost cancelled. In the interaction diagram for C (Figure 5), the levels of the Cl_2 fragment are in a narrow energy window. There is substantial orbital mixing between levels that are of the same C_{2v} symmetry. The long distance between the Cl's lowers the energy of the antibonding σ_u orbital, so that it now lies formally occupied below the HOMO. From the shape of this MO ($3b_1$) in Figure 6 (right), we see a small perturbation due to the mixing of the b_1 levels with the orbitals π_g (dashed lines in the interaction diagram).

The HOMO of B now has become the LUMO of C. This is the origin of the level crossing that produces the energy barrier between B and C. The diminution of the Xe–Cl distance produces a stronger overlap between the fragments, increasing the antibonding interaction between the Xe p_z orbital and the π_u orbital. At the same time, the longer Cl–Cl distance reduces the bonding interaction in the π_u orbital. Together, these two effects raise the energy of the $5a_1$ level, so that it crosses the $4b_1$ level and becomes the LUMO. The HOMO of C is now the antibonding combination between Xe p_x orbital and one of the π_g orbitals of Cl_2, similar in shape to the second HOMO of the B complex (see Figure 6).

Note that the extended Hückel calculations do not predict the correct dissociation pathway for long *a* and *b* (see V for definition of these distances). Instead, the complex dissociates to Xe^{2+} and $2Cl^-$. While this is not correct at large internuclear separations, it gives a reasonable approximation of the electronic distribution in the region of C, and in fact, wherever $5a_1$ is below $4b_1$. The calculated charge distributions for A–D are given in Table I.

Moving from C to the linear molecule D, a second barrier due to another level crossing is encountered. Again we analyze the nature of the orbitals, now in the linear geometry, with the interaction diagram shown in Figure 7.

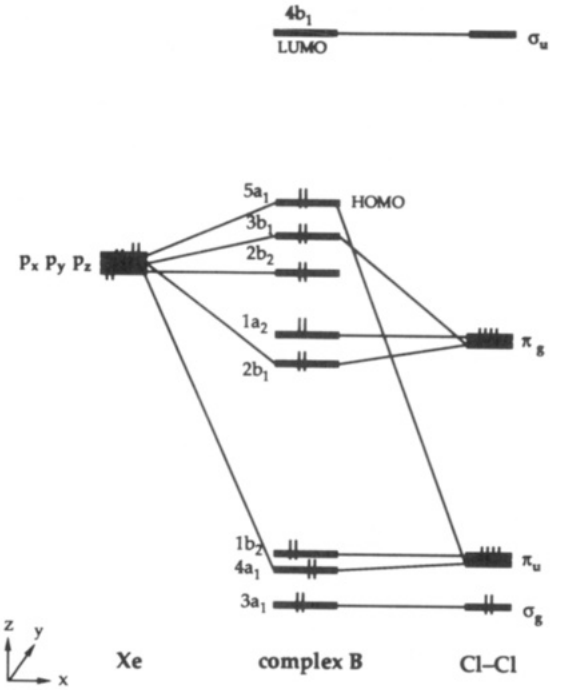

Figure 4. Interaction diagram for complex B in VI.

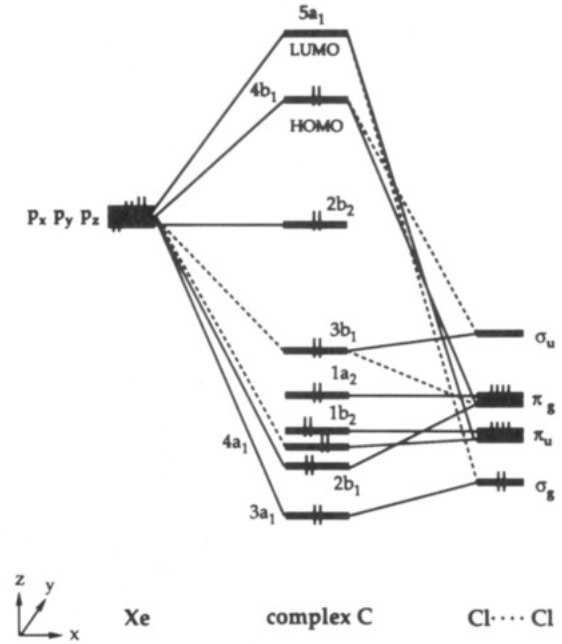

Figure 5. Interaction diagram for geometry C in VI.

Table I. Net Charges on Xe and Cl in Various Geometries

	Xe	Cl		Xe	Cl
A	0.00	0.00	C	1.60	−0.80
B	0.00	0.00	D	1.48	−0.74

The linear molecule in $D_{\infty h}$ presents one strong interaction between the Xe p_x orbital and the σ_u combination of the p_x lone pair on the two chlorines. This interaction produces two σ_u MOs: the LUMO and the lowest occupied MO. This couple makes up two of the three orbitals that bind Cl–Xe–Cl along the axis, in a classical Pimentel three-center four-electron bonding scheme.[13] Qualitatively, the three-center orbitals are shown in VII, and the σ_u orbitals in question are the top and bottom orbitals of this diagram. All the other levels are combinations of lone pairs, as shown in Figure 8.

(13) Pimentel, G. C. *J. Chem. Phys.* **1951**, *19*, 446.

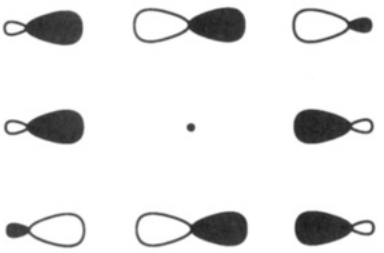

VII

Moving from D to C, the molecule bends from $D_{\infty h}$ to C_{2v} symmetry. The distortion removes the degeneracy of the π levels; the lone pair p_z and p_y orbitals ($2\pi_u$), which represent the HOMO in the linear molecule, now correlate with $5a_1$ and $2b_2$, respectively. $2b_2$ remains unperturbed along the bending path; $5a_1$ mixes with the lone pair on the Cl's of the same symmetry, producing one antibonding level that rises in energy. The LUMO $3\sigma_u$ correlates with $4b_1$ and falls in energy during the bending. This follows from the reduced overlap between the p orbitals (see VIII) and the consequently reduced antibonding interaction.

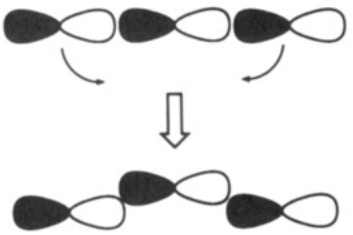

VIII

Thus we expect that the local minimum at geometry C will survive in higher level calculations. Since two level crossings must occur as the geometry goes from the van der Waals to the linear molecule, the two barriers that define structure C cannot be avoided. The dark dots in Figure 2 demarcate the region around species C, where $4b_1$ is filled and $5a_1$ is empty. The impossibility of a transit from the vdW complexes (A, B) to the linear molecule (D) without passing this region is evident.

Is $XeCl_2$ a unique system among all the possible combinations of Ng and X_2? To explore this question, we compute the potential energy surface for selected systems. The necessary condition for the existence of an intermediate such as C is the presence of a large, well-defined region of HOMO–LUMO crossing. This occurs only if the energy of the Ng p orbitals lies close to the energy of the p orbitals of the halogens (see IX). This reduces the likely couples to Xe or Kr with I_2, Br_2, or Cl_2.

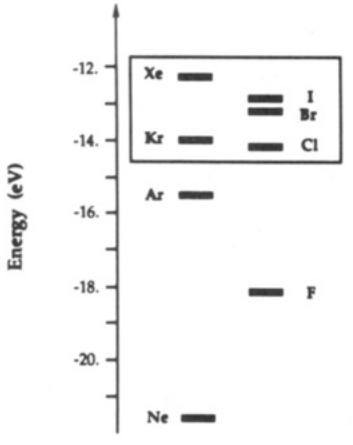

IX

We are able to locate one C-type minimum for each of the six potential energy surfaces (see Table II). The depth of these minima depends on the composition of the HOMO and LUMO, best expressed in terms of the orbitals of Ng and the dihalogen.

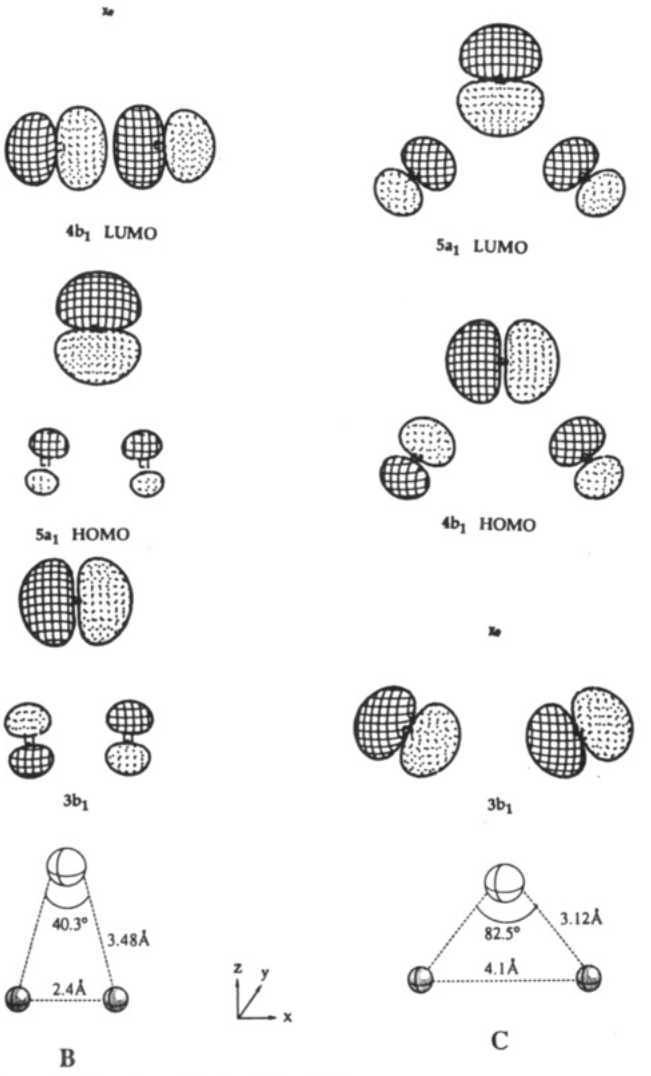

Figure 6. Frontier orbitals of B and C.

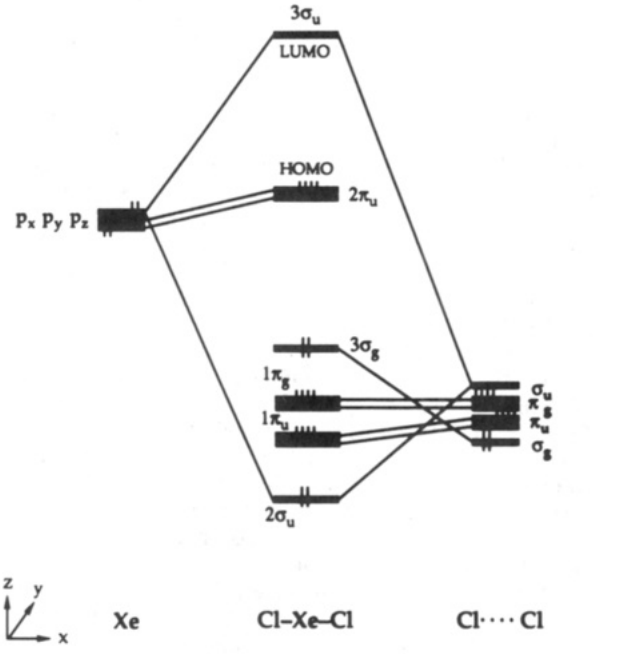

Figure 7. Interaction diagram for linear $XeCl_2$ (D) in VI.

The deepest minimum is obtained when the interaction between the fragments is maximized; this is conveniently measured by the reduced overlap population (last column of Table II). For these geometries, Ng and X_2 participate comparably in the frontier

Table II. Geometries of the Intermediates of Type C for NgX_2 Systems

	Ng-X, Å	X-X, Å	X-Ng-X, deg	HOMO	LUMO	overlap pop.
$Xe-I_2$	3.30	4.07	85	63% p_x + 12% σ_u + 25% π_g	63% p_z + 14% σ_g + 23% π_u	0.159
$Xe-Br_2$	3.24	3.88	73	75% p_x + 11% σ_u + 17% π_g	72% p_z + 11% σ_g + 17% π_u	0.136
$Xe-Cl_2$	3.12	4.10	82	83% p_x + 5% σ_u + 12% π_g	80% p_z + 10% σ_g + 10% π_u	0.097
$Kr-I_2$	3.21	4.27	83	18% p_x + 41% σ_u + 41% π_g	21% p_z + 46% σ_g + 32% π_u	0.101
$Kr-Br_2$	3.00	3.88	80	27% p_x + 32% σ_u + 41% π_g	31% p_z + 42% σ_g + 27% π_u	0.130
$Kr-Cl_2$	3.00	3.99	83	53% p_x + 18% σ_u + 29% π_g	55% p_z + 25% σ_g + 20% π_u	0.141

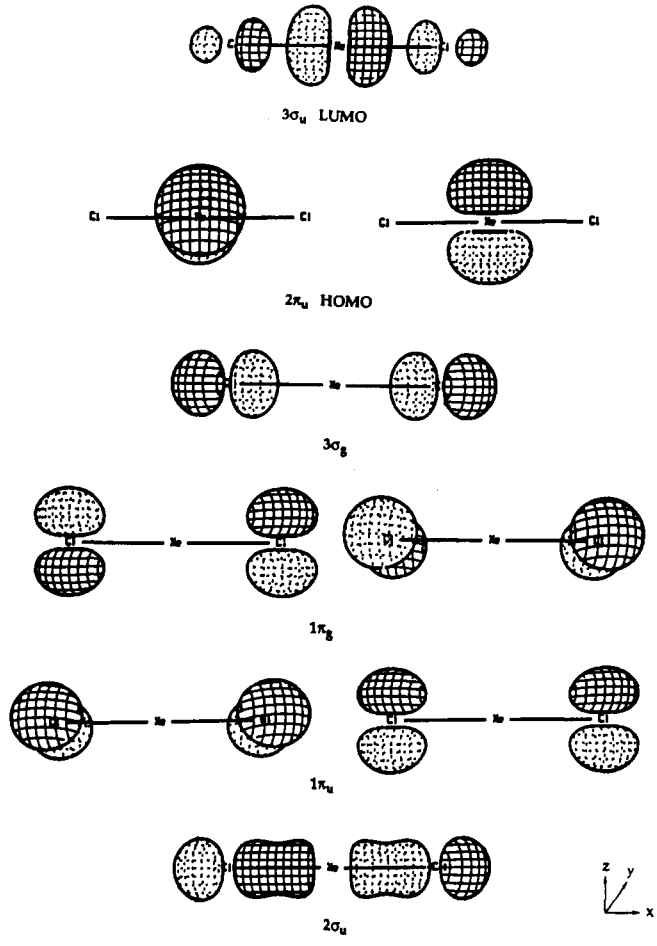

Figure 8. Molecular orbitals of linear $XeCl_2$ (D).

orbitals. The systems XeI_2 and $KrCl_2$ appear to be the most likely candidates for observing this intermediate. As far as we know, there have been no experimental studies of the XeI_2 molecule. $XeBr_2$ has been observed in the β-decay reaction $^{129}IBr_2^- \rightarrow {}^{129}XeBr_2$.[14] For $KrCl_2$, only the vdW isomer has been observed to date.[10] In Figure 9, we show the potential energy surface for the $KrCl_2$ system.

It is interesting to consider how structure C could be observed in the laboratory. One possibility is via stimulated emission pumping. In such an experiment, NgX_2 would first be "pumped" from the ground state to an excited electronic state by one laser. A second laser would be used to "dump" the electronic excited state to region C of the ground-state potential. To explore the possibility of performing such an experiment for $XeCl_2$, we calculated the potential energy curves of three valence-excited states along the path defined in Figure 3.

The excited configurations are as follows: B_2, $(2b_2)^1(5a_1)^1(4b_1)^2$; A_2, $(2b_2)^1(5a_1)^2(4b_1)^1$; B_1, $(2b_2)^2(5a_1)^1(4b_1)^1$. The results shown in Figure 10 indicate that the B_2 and B_1 states have a C-type minimum. There is a singlet–triplet pair for each state, but the extended Hückel method, calculating a simple configuration energy, does not distinguish these.

(14) Perlow, G. J.; Yoshida, H. *J. Chem. Phys.* **1968**, *49*, 1474.

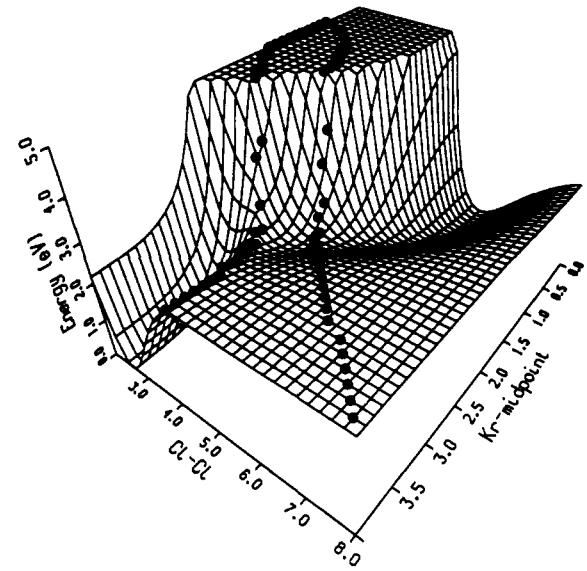

Figure 9. Potential energy surfaces for the $Kr-Cl_2$ system. The black dots mark the geometries at which the crucial $4b_1-5a_1$ level crossing occurs.

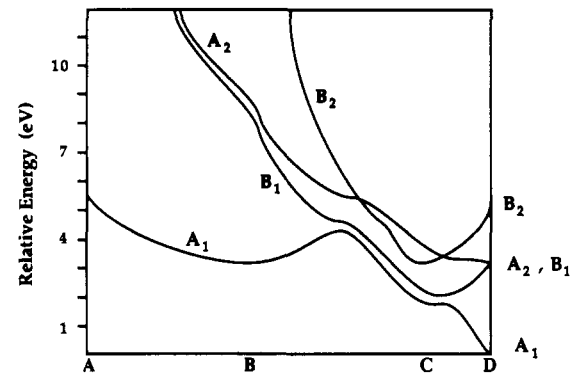

Figure 10. Potential energy curves for the ground state and three valence excited states for $XeCl_2$, along the path defined in Figure 3.

For the B_1 and B_2 excited states, structure C represents the minimum on the potential energy curves. This is very encouraging for the prospects of a stimulated emission pumping experiment. Although it has been observed that the triplet form of the B_1 state, for both $KrCl_2$ and $XeCl_2$, retains its van der Waals geometry,[10] the singlet form may relax quickly to geometry C. Similar geometrical rearrangements may underlie dynamic spectra previously observed for $XeCl_2$.[15]

The B_1 excited states of intermediate C correlate directly with the corresponding states of the van der Waals complex and Cl–Xe–Cl. This is then an allowed reaction, in the context of orbital symmetry arguments. If C can be produced in an excited state, then it should be possible to "dump" down to either geometry C or the linear molecule on the ground-state surface. It is also very interesting to note that C, like the linear molecule D, involves a high degree of charge transfer. If the molecules could be trapped into this geometry, they would have large dipole moments. This

(15) Boinvineau, M.; LeCalvé, J.; Castex, M. C.; Jouvet, C. *Chem. Phys. Lett.* **1986**, *128*, 528; **1986**, *130*, 208.

Table III. Atomic Parameters Used in the Calculation

atom	orbital	H_{ii}, eV	ζ
Ne	2s	-40.96	2.879
	2p	-21.56	2.879
Ar	3s	-27.63	2.585
	3p	-15.76	2.255
Kr	4s	-24.36	2.829
	4p	-13.99	2.442
Xe	5s	-21.21	2.844
	5p	-12.13	2.485
F	2s	-40.0	2.425
	2p	-18.1	2.425
Cl	3s	-26.3	2.183
	3p	-14.2	1.733
Br	4s	-22.07	2.588
	4p	-13.1	2.131
I	5s	-18.0	2.679
	5p	-12.7	2.322

may eventually allow a structural determination by microwave spectroscopy.

Conclusion

In the complete Walsh diagram (Figure 3), we find three minima along a computed reaction pathway from a van der Waals complex to a linear molecule. While the extended Hückel method cannot be used to calculate the heights of the barriers between the three minima, the orbital analysis along the pathway is unambiguous. The presence of two HOMO-LUMO crossings produces two energy barriers, which are expected to be important when Ng and X_2 p-orbital energies are similar, especially for $KrCl_2$ and XeI_2. There is no way that the system can avoid these level crossings.

We believe there will be three possible geometries for $XeCl_2$ and several other NgX_2 species: the van der Waals complex, one intermediate bent state, and the linear molecule. The intermediate state is a surprise and should be the object of an experimental search. We have discussed possible experimental methods to observe both the intermediate geometry and the linear molecule in the gas phase.

Acknowledgment. We thank the Consiglio Nazionale delle Ricerche (CNR, Italy) for the award of a postdoctoral fellowship to D.M.P. and the National Science Foundation for its support through Grant CHE-8912070. We also thank Prof. P. L. Houston for a helpful discussion.

Appendix

For the computations, we use the extended Hückel method,[16] a semiempirical molecular orbital procedure, with weighted H_{ij}'s.[17] The parameters used in the calculations are reported in Table III. The Slater exponents for the noble gases are from ref 18, and the H_{ii} values, from ref 19. The three-dimensional graphics have been carried out by the computer program CACAO, described elsewhere.[20]

Registry No. $XeCl_2$, 13780-38-6; Xe, 7440-63-3; Cl, 7782-50-5.

(16) Hoffmann, R.; Lipscomb, W. N. *J. Chem. Phys.* **1962**, *36*, 2179, 3489. Hoffmann, R. *J. Chem. Phys.* **1963**, *39*, 1397.
(17) Ammeter, J. H.; Bürgi, H.-B.; Thibeault, J. C.; Hoffmann, R. *J. Am. Chem. Soc.* **1978**, *100*, 3686.
(18) Clementi, E.; Raimondi, D. L.; Reinhardt, W. P. *J. Chem. Phys.* **1967**, *47*, 1300.
(19) Moore, C. E. *Natl. Stand. Ref. Data Ser.* (*U.S., Natl. Bur. Stand.*) **1970**, *34*, 4.
(20) Mealli, C.; Proserpio, D. M. *J. Chem. Educ.* **1990**, *66*, 399.

Resonance Raman Structural Characterization and the Mechanism of Formation of Lactoperoxidase Compound III

Songzhou Hu and James R. Kincaid*

Contribution from the Chemistry Department, Marquette University, Milwaukee, Wisconsin 53233. *Received September 11, 1990*

Abstract: Lactoperoxidase compound III (LPO-III) is characterized by resonance Raman spectroscopy with both the Soret and Q-band excitations. The identical spectral patterns observed for LPO-III prepared by the addition of 100-fold hydrogen peroxide to ferric enzyme and by the oxygenation of the ferrous enzyme confirm the formulation of LPO-III as a low-spin dioxygen adduct. The Fe–O_2 stretching vibration (identified at 531 cm^{-1} for the $^{16}O_2$ adduct and 513 cm^{-1} for the $^{18}O_2$ derivative) is the lowest yet reported for an oxygenated heme protein. The anomalous isotopic shift of the ν(Fe–O_2) mode is attributed to vibrational coupling of the Fe–$^{18}O_2$ stretching mode with a heme mode located at 508 cm^{-1}. In addition, the Fe–O–O bending vibration is also observed at 491 cm^{-1}. The study of the ν(Fe–O_2) mode of LPO-III, prepared by different combinations of isotopically labeled peroxides, establishes unambiguously that the ferryl oxygen atom of LPO-II is displaced and the dioxygen fragment of LPO-III is derived from the hydrogen peroxide.

Introduction

Lactoperoxidase, present in mammalian milk, saliva, and tears, is involved in bacterial defense through the oxidation of a thiocyanate ion in the presence of peroxide.[1] The enzyme is composed of a single polypeptide chain with a molecular weight of 78 000, of which about 10% is carbohydrate,[2,3] and a heme group that is extraordinarily tightly bound. Early attempts[4,5] to establish the identity of the prosthetic group used complete pronase digestion of the enzyme. The similarity of the electronic absorption spectrum of the released heme group to that of protoporphyrin IX suggested that a normal protoheme resides at the active site. More recent work based on reductive cleavage of heme with mercaptoethanol in 8 M urea under mild conditions indicated that the prosthetic group is a modified protoporphyrin IX, whose

(1) Pruitt, K. M., Tenovuo, J. O., Eds. *The Lactoperoxidase System: Chemistry and Biological Significance*; Marcel Dekker: New York, 1985.
(2) Carlstrom, A. *Acta Chem. Scand.* **1969**, *23*, 185-213.
(3) Sievers, G. *FEBS Lett.* **1981**, *127*, 253-256.
(4) Sievers, G. *Biochim. Biophys. Acta* **1979**, *579*, 180-190.
(5) Sievers, G. *Biochim. Biophys. Acta* **1980**, *624*, 249-259.

0002-7863/91/1513-7189$02.50/0